nature neuroscience

KIF1A inhibition immortalizes brain stem cells but blocks BDNF-mediated neuronal migration

Aurelie Carabalona, Daniel Jun-Kit Hu & Richard B Vallee

Brain neural stem cells (radial glial progenitors, RGPs) undergo a mysterious form of cell cycle–entrained interkinetic nuclear migration (INM) that is driven apically by cytoplasmic dynein and basally by the kinesin KIF1A, which has recently been implicated in human brain developmental disease. To understand the consequences of altered basal INM and the roles of KIF1A in disease, we performed constitutive and conditional RNAi and expressed mutant KIF1A in E16 to P7 rat RGPs and neurons. RGPs inhibited in basal INM still showed normal cell cycle progression, although neurogenic divisions were severely reduced. Postmitotic neuronal migration was independently disrupted at the multipolar stage and accompanied by premature ectopic expression of neuronal differentiation markers. Similar effects were unexpectedly observed throughout the layer of surrounding control cells, mimicked by Bdnf (brain-derived neurotrophic factor) or Dcx RNAi, and rescued by BDNF application. These results identify sequential and independent roles for KIF1A and provide an important new approach for reversing the effects of human disease.

Development of the cerebral cortex occurs through a series of stages, beginning with RGPs. These stem cells exhibit an unusual form of cell cycle–dependent nuclear oscillation between the apical and the basal regions of the ventricular zone known as INM[1–3]. RGPs are highly proliferative and give rise to most neurons and glia of the cerebral cortex, as well as adult stem cells[4–6]. Neurons generated from asymmetric RGP cell divisions migrate to the subventricular zone (SVZ) and lower intermediate zone (IZ), where they assume a multipolar morphology. After a prolonged residence in this state, they take on a bipolar morphology and migrate along the basal process of neighboring RGP cells to the cortical plate (CP)[4,7]. Mutations in a number of genes responsible for aspects of this complex behavior contribute to a variety of developmental diseases, including periventricular heterotopia, subcortical band heterotopia and lissencephaly[8].

In previous work, our laboratory found that the microtubule motor proteins KIF1A and cytoplasmic dynein are responsible, respectively, for basal and apical INM in rat brain RGP cells[9,10]. Myosin II has also been implicated in this behavior in other systems[11–13], but neither RNAi nor small molecule myosin inhibition has a detectable effect in rat[9]. Mutations in or altered expression of genes encoding the cytoplasmic dynein heavy chain, the dynein regulator LIS1 and factors responsible for recruiting dynein to the G2 nuclear envelope interfered with apical INM and blocked nuclei in a late G2 premitotic state[9,10,14]. Each also resulted in an accumulation of postmitotic neurons in the multipolar state and a block or delay in subsequent migration of bipolar neurons to the CP. Consistent with these effects, dynein and its regulatory factors have been implicated in lissencephaly and microcephaly[15–19].

Similarly, inhibition of basal INM by Kif1a RNAi might also be expected to have a marked influence on subsequent brain development. Neuronal distribution was, in fact, altered[9,20], although direct effects on migration remain unexamined. Brain size is reduced in a Kif1a null mouse[21], and human KIF1A mutations have been found to cause a number of neuropathies[22–28]. The relationship between the brain malformations and the specific roles of KIF1A are poorly understood.

We sought to determine the consequences of altered basal INM on RGP cell cycle progression and neurogenesis and to test for potential effects on subsequent neuronal migration. To address these issues, we used *in utero* electroporation to express shRNAs and a KIF1A mutant cDNA in embryonic rat brain. Blocking basal INM had little effect on RGP cell cycle progression, resulting in a perpetuation of stem cell–like behavior. However, neurogenic divisions were markedly reduced and the multipolar stage was blocked, although progressive expression of later differentiation markers persisted. These effects were also propagated non-autonomously in surrounding control cells, phenocopied by doublecortin or Bdnf knockdown, and reversed by BDNF application. Our data reveal marked phenotypic effects of Kif1a inhibition, with important consequences for understanding and rescuing brain developmental deficits.

RESULTS

RGP cell cycle progresses independently of basal migration

In previous work, we found that inhibition of apical INM inhibits RGP mitotic entry[9]. The effect of altered basal migration on cell cycle progression has not been examined, though we did observe Kif1a RNAi to increase the percentage of Pax6+ RGP cells[9] and to decrease the number of intermediate progenitors (scramble, 16.6 ± 3.6%, $n = 4$; Kif1a shRNA, 3.92 ± 2.05%, $P = 0.0286$, $n = 4$; **Supplementary Fig. 1**). To test for cell cycle effects, we introduced Kif1a shRNAs into embryonic day 16 (E16) rat brain progenitor cells by *in utero* electroporation, sectioned brains at E20 and stained for cell cycle markers.

Department of Pathology and Cell Biology, Columbia University, New York, New York, USA. Correspondence should be addressed to A.C. (ac3588@cumc.columbia.edu) or R.B.V. (rv2025@cumc.columbia.edu).

Received 8 June 2015; accepted 1 December 2015; published online 11 January 2016; doi:10.1038/nn.4213

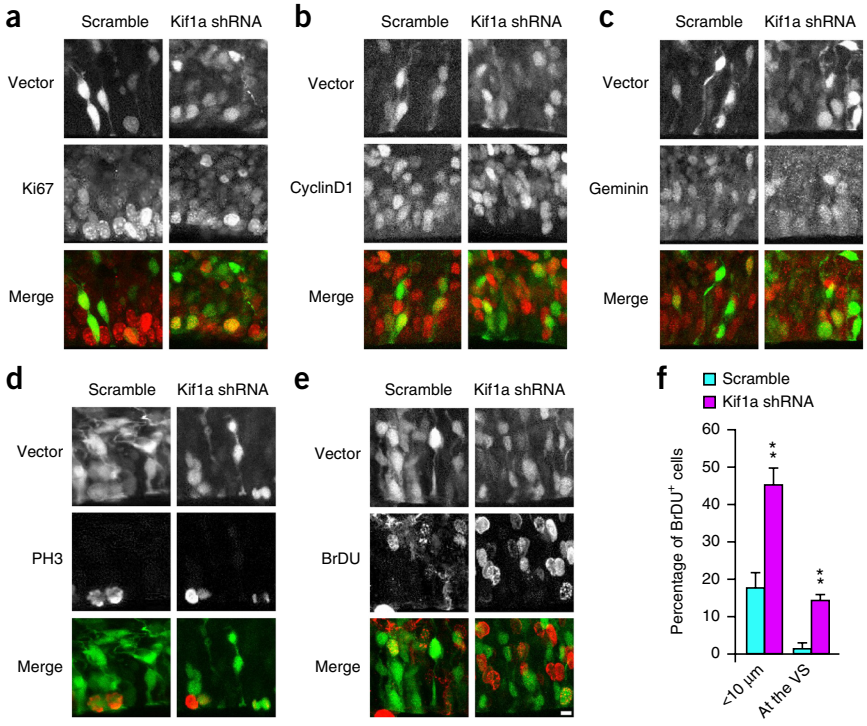

Figure 1 Kif1a RNAi inhibition of basal nuclear migration in RGP cells has no effect on cell cycle progression. (**a**–**e**) E16 rat brains were subjected to *in utero* electroporation with the pRNAT vector expressing either scrambled or Kif1a shRNAs. Brains were then fixed at E20 and stained with cell cycle markers as indicated. There was no substantial change in the percent of cycling (Ki67), mitotic (PH3), G1 (CyclinD1), S (BrDU after 20 min pulse label) or G2 (Geminin) cells. Scale bars represent 15 µm. (**f**) The percentage of BrDU-positive nuclei after 20-min pulse label located less than 10 µm from or at the ventricular surface (VS) greatly increased in RGP cells expressing Kif1a RNAi (<10 µm: scramble, 17.66 ± 4%, $n = 3$; Kif1a shRNA, 45.19 ± 4.2%, $n = 4$, $P = 0.0079$; at the VS: scramble, 1.58 ± 1.4%, $n = 3$; Kif1a shRNA, 14.4 ± 1.4%, $n = 4$, $P = 0.0079$). $^{**}P < 0.01$. Error bars represent mean ± s.d.

A comparable percentage of control and Kif1a knockdown RGP cells expressed Ki67 (scramble, 77.48 ± 4.9%, $n = 3$; Kif1a shRNA, 78.08 ± 6.4%, $P = 0.9$, $n = 3$; **Fig. 1a**). This suggests that Kif1a has no gross effect on the fraction of cycling cells, although a subpopulation in each case escaped the cell cycle (scramble, 77.48 ± 4.9%, $n = 3$; Kif1a shRNA, 78.08 ± 6.4%, $P = 0.9$, $n = 3$; **Fig. 1a**). To our surprise, there was little-to-no effect on the percentage of Kif1a shRNA–expressing RGP cells expressing cyclin D1 (G1 phase; scramble, 34.59 ± 4.1%, $n = 3$; Kif1a shRNA, 35.67 ± 2.9%, $P = 0.7$, $n = 3$; **Fig. 1b**), geminin (S/G2 phases; scramble, 45.99 ± 3.2%, $n = 3$; Kif1a shRNA, 37.14 ± 4.7%, $P = 0.1$, $n = 3$; **Fig. 1c**) or phospho-histone H3 (late G2/M phases; scramble, 5.44 ± 1.5%, $n = 3$, Kif1a shRNA, 4.65 ± 1.2%, $P = 0.8$, $n = 4$; **Fig. 1d**). We also investigated the effect of Kif1a RNAi on S phase by BrDU pulse labeling. According to this measure, 18% of cells were in S phase, a somewhat lower value than for controls, but one that strongly supports continued cell cycle progression (scramble, 26.22 ± 3.5%, $n = 3$; Kif1a shRNA, 17.91 ± 6.06%, $P = 0.2$, $n = 4$; **Fig. 1e**). Notably, the majority of nuclei in BrDU$^+$ Kif1a-depleted cells were located within 10 µm of the apical brain surface (**Fig. 1f**), indicating that nuclei can enter S phase without reaching the outer ventricular zone (VZ). The morphology of these cells looked no different than that of control cells in the VZ (**Fig. 1e**), with a basal process extending to the pial surface of the cortex. These results indicate that RGP cells can progress through the entire cell cycle while remaining close to the ventricular surface (VS). We note that, although basal INM is severely inhibited, some nuclei are located as far as 25 µm from the VS (see below), probably reflecting cell body crowding[29] or incomplete Kif1a knockdown.

To visualize cell cycle progression directly, we imaged live brain slices beginning 3 d after electroporation (to ensure adequate knockdown) for up to 40 h, which was sufficient to enable tracking through two mitotic events (based on 20-h cell cycle estimated from mitotic index; **Fig. 1d**). Nuclei in control RGP cells exhibited migration in both apical and basal directions, undergoing mitosis at the apical surface as expected (**Fig. 2a**). In Kif1a shRNA–expressing cells, nuclei could be followed throughout the end of apical migration and mitosis at the VS. As expected, the reformed nuclei were deficient in basal migration (**Fig. 2b**). Some exhibited short departures from the VS (**Fig. 2c**,**d**), again possibly reflecting incomplete Kif1a knockdown or cell body crowding. Following cytokinesis, however, most of the reformed nuclei remained at the VS and then divided again, which is direct evidence for persistent progression through the cell division cycle (**Fig. 2b**).

Kif1a RNAi results in a decrease in neurogenic divisions

These results argue strongly against a role for altered cell cycle progression in the increased ratio of progenitors resulting from Kif1a RNAi[9]. We therefore examined mitotic cells for the ratio of symmetric (proliferative; **Fig. 2c** and **Supplementary Movie 1**) versus asymmetric (neurogenic) divisions (**Fig. 2d** and **Supplementary Movie 2**). For this purpose, we monitored mitosis live and scored cells for cytokinetic plane, centrosome position (using DsRed-centrinII), and morphology and migration behavior of the progeny cells (**Fig. 2c**,**d**). By these indicators, Kif1a RNAi caused a marked increase in the percent of symmetric divisions compared to control (**Fig. 2e**,**f**). This result is consistent with the increase in Pax6-positive Kif1a shRNA–expressing cells, although the absolute fraction of these cells relative to total was too low (9.3 ± 2%, $n = 5$) to detect overall changes in Pax6-positive cell density or VZ thickness.

Kif1a RNAi blocks multipolar-bipolar transition in neurons

Despite the limited consequences of altered basal INM on cell cycle progression, Kif1a RNAi caused an accumulation of cells in the SVZ/ IZ (**Fig. 3a**)[9,20]. Cells in this region of control brains typically assume a multipolar morphology before reorganizing to a bipolar form and migrating toward the CP. The Kif1a shRNA–accumulated neurons were largely multipolar, suggesting a potential failure in the multipolar-bipolar transition (**Fig. 3a**,**b**). The multipolar stage has been reported to last >24 h[7], but can be detected by long-term live imaging[9]. Control multipolar neurons were seen to transition to a bipolar morphology (**Fig. 3c** and **Supplementary Movie 3**). In contrast, none of the multipolar Kif1a-depleted neurons converted to the bipolar morphology over a comparable period, supporting the notion that there is a block at this stage of morphogenesis (**Fig. 3d**,**e** and

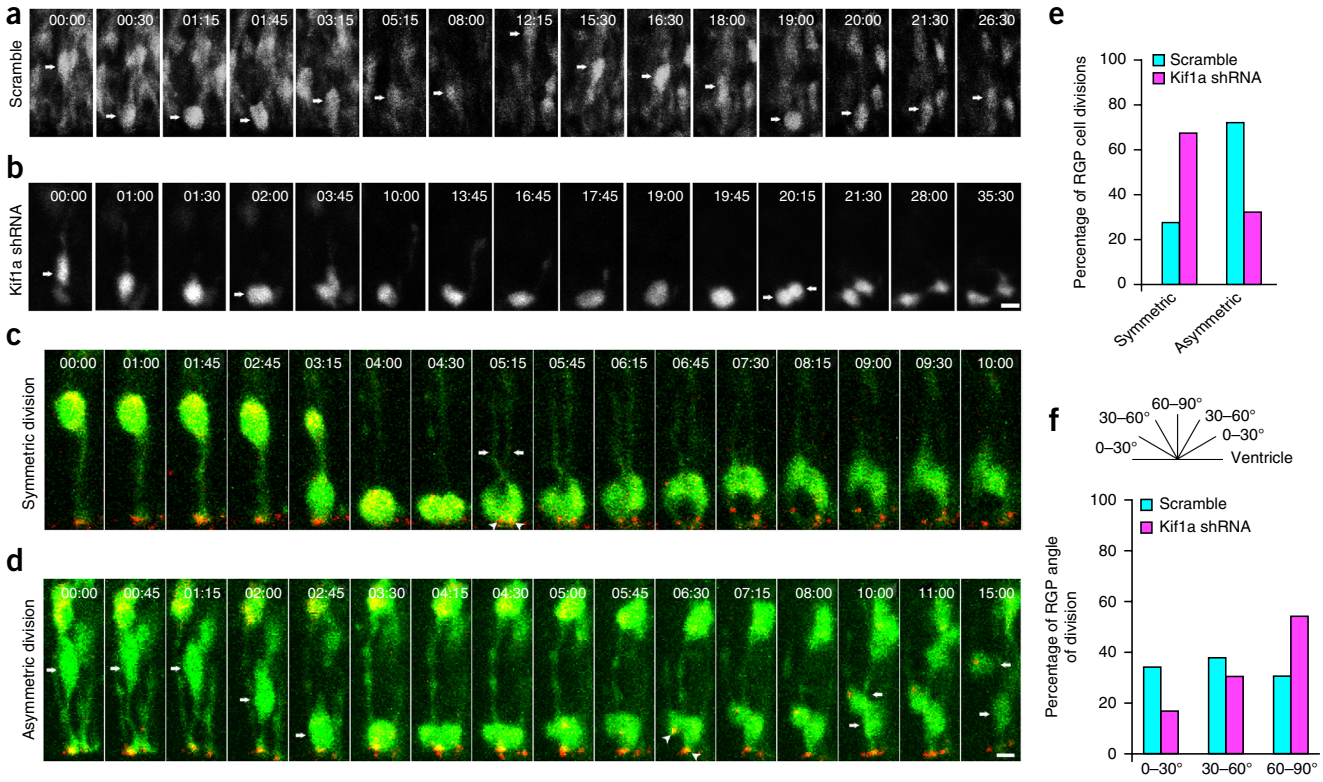

Figure 2 RGP cells exhibit persistent symmetric divisions despite basal migration arrest. Brain slices prepared following *in utero* electroporation with Kif1a or scrambled shRNAs were cultured at E19 and monitored by live imaging for 40–45 h. Time lapse duration shown (in h:min) was varied as needed to include major INM events. (**a**) Control RGP cell (arrow) underwent two cycles of INM, each time exhibiting basal and then apical nuclear migration, followed by mitosis at the ventricular surface of the brain slice (1:45; 20:00). (**b**) Nucleus of Kif1a knockdown RGP (arrow) initially underwent apical INM and divided (2:00). The one nucleus that stayed in the image focal plane remained at the ventricular surface for ~18 h before dividing again (20:15; arrows). (**c**,**d**) RGP cells coexpressing Kif1a shRNA and DsRed-centrin II were able to divide either symmetrically (**c**) to form two RGP cells or asymmetrically (**d**) to form a RGP cell and a neuron/neuronal progenitor. Daughter RGP cells were identified by the presence of an apical process (arrows) and an apically sequestered centrosome (arrowheads) at the ventricular surface of the brain slice. Newly born neurons were identified by movement toward the SVZ (arrows), absence of an apical process and centrosomal movement away from the ventricular surface (arrowheads). (**e**) Quantification of the symmetric versus asymmetric RGP divisions based on the average of every recorded cell, pooled from multiple examples of live imaging (see **c** and **d**), revealed that Kif1a shRNA caused a severe shift toward symmetric divisions (symmetric: scramble, 28%; Kif1a shRNA, 68%; asymmetric: scramble, 72%; Kif1a shRNA, 32%; $n = 25$ cells per condition). (**f**) Quantification of cleavage plane orientation (based from the average of every recorded cell, pooled from multiple live imaging events) indicates a similarly marked shift to a horizontal cleavage plane orientation (0–30°: scramble, 33.33%; Kif1a shRNA, 16.66%; 30–60°: scramble, 36.66%; Kif1a shRNA, 30%; 60–90°: scramble, 30%; Kif1a shRNA, 53.33%; $n = 30$ cells per condition). Scale bars represent 20 μm (**a**,**b**) and 15 μm (**c**,**d**).

Supplementary Movie 4). Nonetheless, a few bipolar Kif1a-depleted neurons could be detected in the IZ and CP. These neurons were able to migrate normally toward the CP at similar rates to those of control neurons (data not shown). These results suggest that KIF1A is not required for bipolar neuronal migration, but is essential for regulating the switch to the bipolar migratory morphology.

Cell fate of arrested neurons

To characterize the effects of Kif1a RNAi on further neuronal differentiation, we stained brain sections with a number of neuronal markers. Tbr1 is normally expressed in postmitotic projection neurons[30,31]. In E20 control brains, only bipolar neurons located in the upper IZ and CP expressed this marker (**Fig. 3f**). Multipolar neurons in the SVZ and lower IZ did not express Tbr1. However, brains subjected to Kif1a RNAi exhibited Tbr1 staining in most of the multipolar neurons accumulated in the SVZ and lower IZ (**Fig. 3g**). This suggests that the sequence of neuronal gene expression persists in these cells, despite the arrest in migration.

To extend our cell fate analysis to later neuronal markers, we used the stronger CAG promoter to better visualize shRNA-expressing cells (**Supplementary Fig. 2**) and followed brain development postnatally. By postnatal day 7 (P7), all cells transfected with control shRNA had reached the superficial cortical layers (**Fig. 4a**),and expressed the neuronal marker NeuN (**Fig. 4b**) and the superficial layer marker CDP (**Fig. 4d**). In contrast, Kif1a-depleted cells remained as a broad subcortical band in what had become the white matter (**Fig. 4a**), and remained positive for NeuN and CDP (**Fig. 4c–e**). Similar to knockdown of other genes[32], some of these neurons seemed to remain multipolar, but with very short processes, whereas others had no processes, and their subsequent fate was uncertain.

Non-cell-autonomous effects of Kif1a RNAi

A particularly surprising observation was the effect of Kif1a RNAi on surrounding non-transfected cells. At E20, a large proportion of these cells in the SVZ and lower IZ were also multipolar and expressed Tbr1 (**Fig. 3g**). Furthermore, by P7, the heterotopic band of cells in the white matter expressed NeuN and CDP (**Fig. 4f–h**). Assuming that Kif1a expression itself was unaltered in these cells, the heterotopic band must be caused by a non-cell-autonomous effect of the Kif1a knockdown. In contrast, knockdown of the dynein-related genes

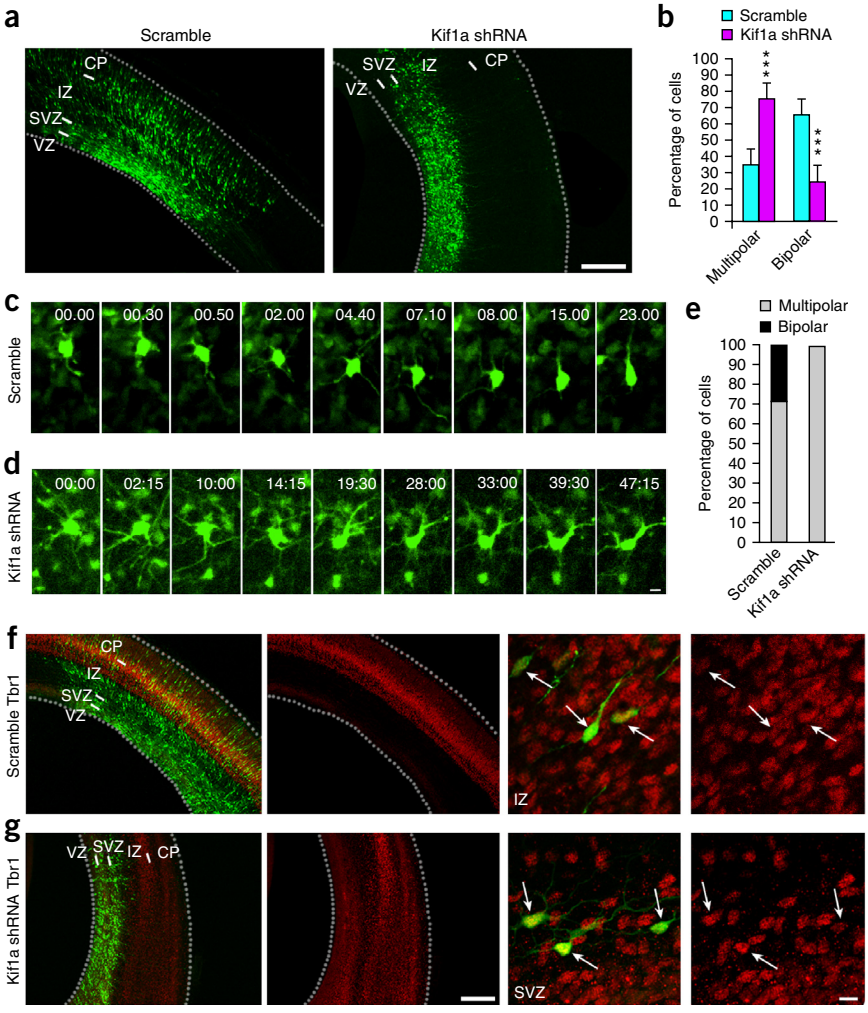

Figure 3 Cell-autonomous and non-autonomous effects in neuronal morphogenesis and gene expression. Histological analysis and live imaging of rat brains *in utero* electroporated with Kif1a and scrambled shRNA vectors at E16. (**a**) Coronal sections of E20 rat brains showing an accumulation of multipolar neurons in the SVZ/lower IZ in Kif1a knockdown compared with control. (**b**) Quantification of the number of multipolar versus bipolar E20 neurons in the cortex in Kif1a knockdown compared with control (multipolar: scramble, 34.75 ± 6.2%; Kif1a shRNA, 75.15 ± 9.5%, $P < 0{,}0001$; bipolar: scramble, 62.25 ± 6.2%; Kif1a shRNA, 24.85 ± 9.5%, $P < 0{,}0001$; $n = 10$ scramble and 9 Kif1a shRNA). (**c**,**d**) E20 brain slices were cultured for ~40 h during which we monitored, in the SVZ and lower IZ, control multipolar cells converting to a bipolar morphology by 15 h (**c**), and the absence of the transition in Kif1a knockdown cells (**d**). (**e**) Quantification of live analysis. During ~40 h of imaging, ~30% of all recorded control multipolar cells (pooled from multiple live imaging events), located in the IZ, converted to a polar migratory morphology, whereas none of the Kif1A knockdown cell showed this behavior (scramble: $n = 51$ cells, 70.6% multipolar and 29.4% bipolar; Kif1a shRNA, $n = 16$ cells, 100% multipolar). (**f**,**g**) Low- and high-magnification coronal sections of Kif1a versus control rat brains immunostained at E20 for the neuronal marker Tbr1. As expected, Tbr1 staining was detected in bipolar neurons (arrows) in the upper IZ and CP (**f**). However, Kif1a RNAi resulted in ectopic Tbr1 staining in transfected as well as surrounding non-transfected cells in the SVZ and lower IZ. ***$P < 0.001$. Error bars represent mean ± s.d. Scale bars represent 100 µm (**a**, left two panels in **f**,**g**) and 15 µm (**c**,**d** and right two panels in **f**,**g**).

Bicd2, *Cenpf* and *Nup133*, which cause similar accumulation of multipolar cells in the SVZ, showed no indication of inducing late neuronal marker expression (**Supplementary Fig. 3a–c**). These results indicate that the non-cell-autonomous effect is Kif1a RNAi specific and not a general consequence of multipolar arrest.

To test further for a non-cell-autonomous effect of Kif1a RNAi, we performed sequential *in utero* electroporations[33]. In contrast with co-electroporation, most cells appeared to be singly transfected after sequential electroporation (co-electroporation: 45.17 ± 7.8%, $n = 5$; sequential electroporation: 24.72 ± 2.5%, $n = 5$; $P = 0.0025$; **Supplementary Fig. 4**). Cells expressing either GFP-scrambled or cytoplasmic RFP were comparably distributed throughout the IZ and CP 4 d after sequential electroporation (**Fig. 5a**). In contrast, sequential electroporation with pCAG-RFP and Kif1a shRNA caused both classes of cell to accumulate in the SVZ and lower IZ with a multipolar morphology and to express ectopic Tbr1 (**Fig. 5b**), further evidence for a non-cell-autonomous effect of Kif1a RNAi.

Sequential electroporation has previously revealed a non-cell-autonomous effect of doublecortin (Dcx) RNAi on the migration of nearby control neurons[33]. This observation and a reported interaction between Kif1a and Dcx raise the possibility of a functional relationship[20]. To test for additional common features, we performed Dcx RNAi and stained for Tbr1 (**Supplementary Fig. 3d**). Similar to Kif1a, Dcx knockdown cells accumulated in the SVZ and lower IZ and, along with nearby non-transfected cells, exhibited ectopic Tbr1 expression.

Relationship between Kif1a roles in RGP cells and neurons

We observed no apparent effect of Kif1a shRNA–expressing cells on INM in nearby control RGP cells (**Fig. 5c**). This suggests that the non-autonomous Kif1a RNAi effects are specific to postmitotic neurons.

We also knocked down Kif1a either specifically in RGP cells (BLBP; **Fig. 6a**,**b**) or neurons (NeuroD; **Fig. 6c**,**d**). By 4 d after electroporation, Kif1a knockdown in RGP cells caused the expected accumulation of nuclei near the VS (**Fig. 6b**). However, there was no effect on morphology or Tbr1 expression in neuronal progeny cells in the SVZ and IZ or on nearby non-transfected neurons (**Fig. 6a**). In contrast, Kif1a knockdown using the *Neurod1* promoter caused accumulation of both transfected and non-transfected neurons in the multipolar state with ectopic Tbr1 expression (**Fig. 6c**), as we had seen for constitutive Kif1a RNAi (**Fig. 3**). Together, these results support distinct early and late roles for KIF1A in brain development, and attribute the non-cell-autonomous effects of RNAi with physiological changes in nearby neurons.

Altered RGP morphology, as observed from Filamin-A knockdown, inhibits glial-guided neuronal migration, resulting in periventricular heterotopia[34]. To test for this form of non-cell-autonomous effect, we stained Kif1a knockdown cells for vimentin, but observed

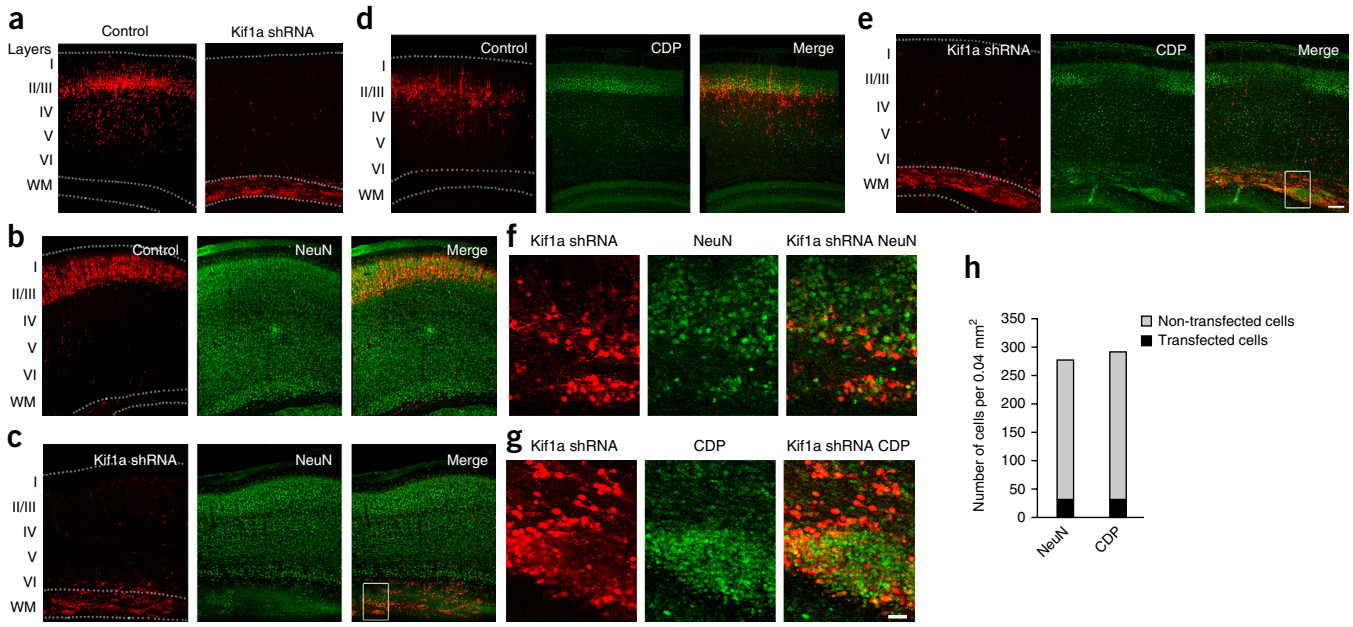

Figure 4 Cell autonomous and non-autonomous effects on neuronal markers at P7. E16 rat brains were electroporated *in utero* using pCAG-RFP alone as a control or with Kif1a shRNA subcloned into the U6 vector to ensure that expression would persist in postnatal pups. Histological analysis of brains was carried out at P7. (**a**) Representative neocortical sections showing the laminar position of transfected cells. In control brain, RFP-positive cells are mainly found in layers II/III/IV of the neocortex. In contrast, in Kif1a shRNA brains, RFP-positive cells remained in the white matter (WM) located in a heterotopic band near the ventricular surface. (**b**–**e**) Immunostaining for the neuronal marker NeuN (**b**) and the upper cortical layer marker CDP (**d**) was observed near the pial surface in control transfected brain, but near the ventricular surface in Kif1a knockdown brain (**c**,**e**). (**f**,**g**) High-magnification views of the boxed sections in merged images for control versus Kif1a knockdown brains show both transfected and non-transfected cells expressing NeuN (**f**) and CDP (**g**). (**h**) Ratio of transfected to non-transfected NeuN$^+$ and CDP$^+$ neurons in a surface area of 0.04 mm^2 (transfected cells: NeuN, 31.25; CDP, 32.28; non-transfected cells: NeuN, 244.25; CDP, 259.57). Scale bars represent 100 μm (**a**–**e**) and 25 μm (**f**,**g**).

no apparent effect on RGP structure (**Supplementary Fig. 5a**). Furthermore, the basal processes of Kif1a depleted RGP cells were found to remain extended to the pial surface of the cortex (**Supplementary Fig. 5b**).

The R18W human mutation alters INM and neuronal migration

A somatic autosomal dominant mutation in human *KIF1A* identified by deep sequencing was recently reported to cause frontal pachygyria[27], consistent with a defect in neuronal migration. To test the effects

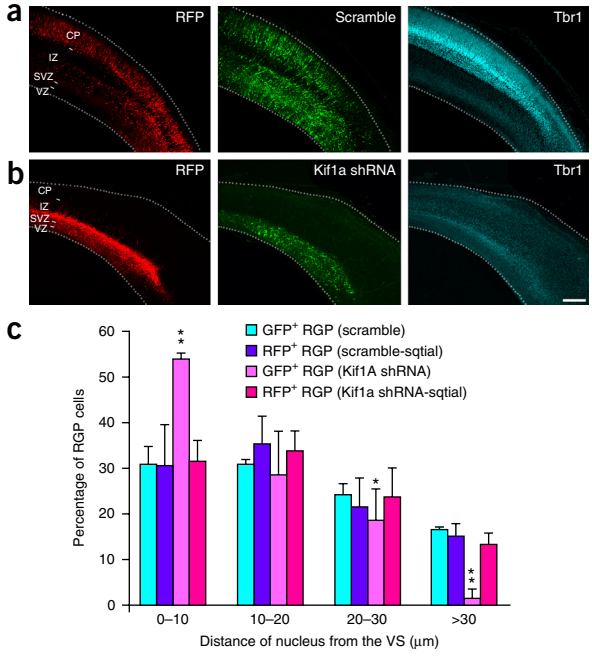

Figure 5 Sequential electroporation test for non-cell-autonomous effects of Kif1a RNAi. (**a**) E16 rat brains were electroporated with pCAG-RFP and 30 min later with GFP-scrambled plasmid. Brain sections were prepared 4 d after electroporation and showed similar distributions of RFP$^+$ and GFP$^+$ cells through the cortex and normal Tbr1 staining. (**b**) In contrast, sequential electroporation of pCAG-RFP followed by GFP-Kif1a shRNA resulted in an accumulation of both RFP$^+$ and GFP$^+$ neurons in the SVZ and lower IZ. Immunostaining against Tbr1 revealed that neurons in the SVZ and lower IZ expressing only RFP were ectopically positive for Tbr1, similar to the neighboring Kif1a-depleted cells. (**c**) Quantification of the nuclear distance from the VS for RGP cells after electroporation of scrambled or Kif1a RNAi alone or RFP$^+$ RGP cells after sequential electroporation of GFP-scrambled (scramble-sqtial) or Kif1a RNAi (Kif1a shRNA-sqtial). Nuclear distribution of RFP$^+$ RGP cells was not significantly altered after sequential electroporation of GFP-Kif1a RNAi (0–10: scramble, 30.14 ± 2.4%; scramble-sqtial, 29.96 ± 8.7%; Kif1a shRNA, 51.61 ± 2%; Kif1a shRNA-sqtial, 30.84 ± 4.4%; 10–20: scramble, 29.97 ± 1%; scramble-sqtial, 34.50 ± 6%; Kif1a shRNA, 27.09 ± 6%; Kif1a shRNA-sqtial, 32.94 ± 4.5%; 20–30: scramble, 23.52 ± 1.4%; scramble-sqtial, 20.86 ± 6.3%; Kif1a shRNA, 18.51 ± 4.7%; Kif1a shRNA-sqtial, 23.13 ± 6.3%; >30: scramble, 15.87 ± 1.2%; scramble-sqtial, 14.67 ± 2.7%; Kif1a shRNA, 1.7 ± 1.2%; Kif1a shRNA-sqtial, 13.07 ± 2.2%; $n = 6$ for each), suggesting Ki1a depletion does not have a non-cell-autonomous effect on INM in neighboring RGP cells (0–10: $P = 0.0022$ for scramble versus Kif1a shRNA, $P = 0.9004$ for scramble-sqtial versus Kif1a shRNA-sqtial; 10–20: $P = 0.0931$ for scramble versus Kif1a shRNA, $P = 0.6688$ for scramble-sqtial versus Kif1a shRNA-sqtial; 20–30: $P = 0.0260$ for scramble versus Kif1a shRNA, $P = 0.7316$ for scramble-sqtial versus Kif1a shRNA-sqtial; >30: $P = 0.0022$ for scramble versus Kif1a shRNA, $P = 0.2229$ for scramble-sqtial versus Kif1a shRNA-sqtial). Error bars represent mean ± s.d. $^*P < 0.05$, $^{**}P < 0.01$. Scale bar represents 100 μm (**a**,**b**).

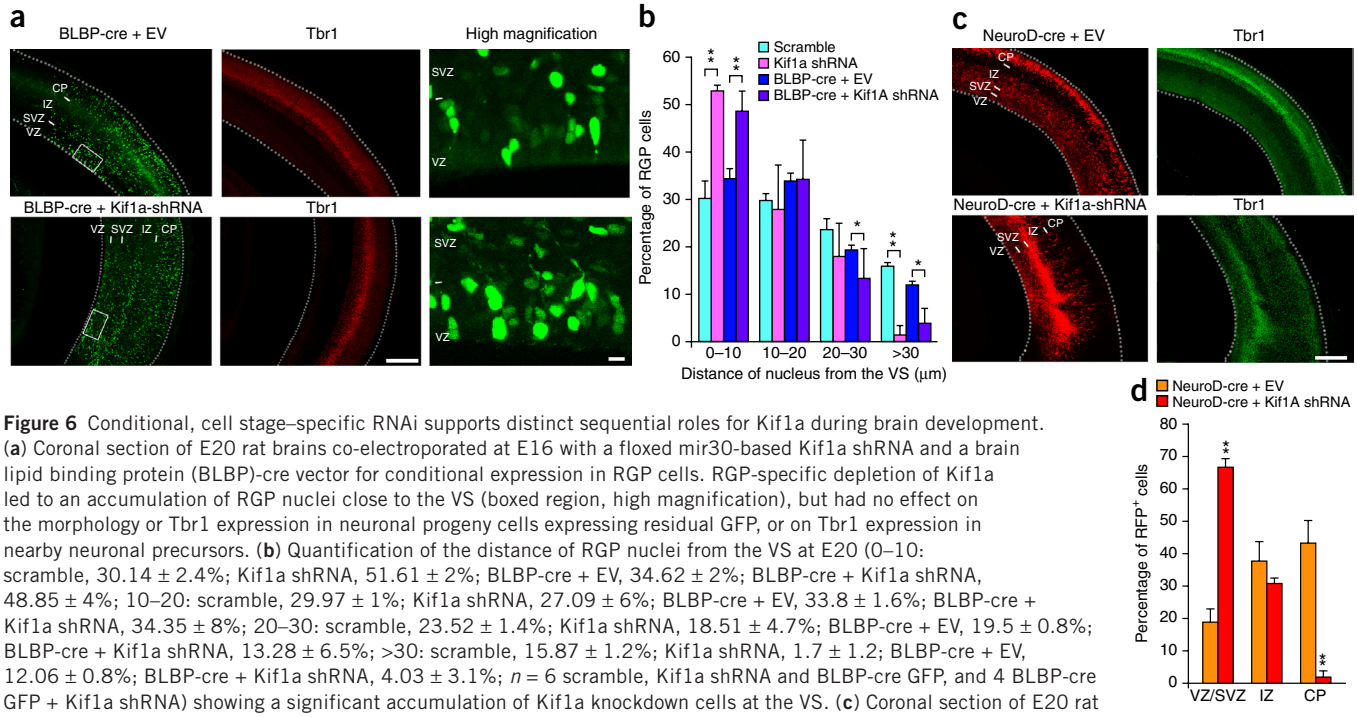

Figure 6 Conditional, cell stage–specific RNAi supports distinct sequential roles for Kif1a during brain development. (**a**) Coronal section of E20 rat brains co-electroporated at E16 with a floxed mir30-based Kif1a shRNA and a brain lipid binding protein (BLBP)-cre vector for conditional expression in RGP cells. RGP-specific depletion of Kif1a led to an accumulation of RGP nuclei close to the VS (boxed region, high magnification), but had no effect on the morphology or Tbr1 expression in neuronal progeny cells expressing residual GFP, or on Tbr1 expression in nearby neuronal precursors. (**b**) Quantification of the distance of RGP nuclei from the VS at E20 (0–10: scramble, 30.14 ± 2.4%; Kif1a shRNA, 51.61 ± 2%; BLBP-cre + EV, 34.62 ± 2%; BLBP-cre + Kif1a shRNA, 48.85 ± 4%; 10–20: scramble, 29.97 ± 1%; Kif1a shRNA, 27.09 ± 6%; BLBP-cre + EV, 33.8 ± 1.6%; BLBP-cre + Kif1a shRNA, 34.35 ± 8%; 20–30: scramble, 23.52 ± 1.4%; Kif1a shRNA, 18.51 ± 4.7%; BLBP-cre + EV, 19.5 ± 0.8%; BLBP-cre + Kif1a shRNA, 13.28 ± 6.5%; >30: scramble, 15.87 ± 1.2%; Kif1a shRNA, 1.7 ± 1.2; BLBP-cre + EV, 12.06 ± 0.8%; BLBP-cre + Kif1a shRNA, 4.03 ± 3.1%; $n = 6$ scramble, Kif1a shRNA and BLBP-cre GFP, and 4 BLBP-cre GFP + Kif1a shRNA) showing a significant accumulation of Kif1a knockdown cells at the VS. (**c**) Coronal section of E20 rat brains co-electroporated with a floxed mir30-based Kif1a shRNA and a NeuroD-cre vector for conditional expression in neurons. Neuron-specific depletion of Kif1a led to an accumulation of the majority of transfected neurons at the multipolar stage in the SVZ and lower IZ. The non-cell-autonomous effect of Kif1a RNAi on surrounding cells was similarly preserved as determined by anti-Tbr1 staining. (**d**) Quantification of RFP$^+$ cell distribution in the cortex at E20 (VZ and SVZ: NeuroD-cre + EV, 19.12 ± 3.7%; NeuroD-cre + Kif1a shRNA, 67.15 ± 2.6%; IZ: NeuroD-cre + EV, 37.66 ± 6.1%; NeuroD-cre + Kif1a shRNA, 31.21 ± 1.3%; CP: NeuroD-cre + EV, 43.21 ± 7.4%; NeuroD-cre + Kif1a shRNA, 1.63 ± 2%; $n = 6$ NeuroD-cre + EV and 5 NeuroD-cre + Kif1a shRNA) showing a significant increase of Kif1a knockdown cells in SVZ and lower IZ. $^*P < 0.05$, $^{**}P < 0.01$ (0–10: $P = 0.0022$ for scramble versus Kif1a shRNA, and $P = 0.0095$ for BLBP-cre GFP versus BLBP-cre GFP + Kif1a shRNA; 10–20: $P = 0.0931$ for scramble versus Kif1a shRNA, and $P > 0.9999$ for BLBP-cre GFP versus BLBP-cre GFP + Kif1a shRNA; 20–30: $P = 0.2333$ for scramble versus Kif1a shRNA, and $P = 0.0260$ for BLBP-cre GFP versus BLBP-cre GFP + Kif1a shRNA; >30: $P = 0.0022$ for scramble versus Kif1a shRNA, and $P = 0.0190$ for BLBP-cre GFP versus BLBP-cre GFP + Kif1a shRNA; VZ/SVZ, $P = 0.0043$; IZ, $P = 0.0823$; CP, $P = 0.0043$). Error bars represent mean ± s.d. Scale bars represent 100 μm (**a**, left two panels; **c**) and 15 μm (high magnification in **a**).

of this mutation in rat, we expressed a human cDNA encoding the same missense mutation, p.R18W, by *in utero* electroporation into E16 rat brain. We observed no defect from control wild-type human KIF1A expression (KIF1A-FL; **Fig. 7a**)[9]. p.R18W expression, however, resulted in the accumulation of multipolar neurons in the SVZ and lower IZ with very few bipolar neurons (**Fig. 7b**,**c**), consistent with the effects that we observed for Kif1a RNAi. The mutant protein also induced Tbr1 expression in most of the transfected multipolar neurons and nearby non-transfected cells (**Fig. 7b**). We also observed clear accumulation of RGP nuclei at the VS of the brain, consistent with a block in basal INM (**Fig. 7b**,**d**). These data reveal that the human mutation affects both of the functions altered by RNAi.

BDNF and KIF1A are essential for neuronal migration

How KIF1A contributes to postmitotic neuronal migration is not understood. It has been found to participate in vesicular transport in non-neuronal and neuronal cells[21,35,36] and contributes to dense-core vesicle transport[37]. Thus, altered Kif1a expression or activity might potentially interfere with growth factor transport and secretion. Vesicles containing the neurotrophin Bdnf, in particular, have been suggested to be under Kif1A control[38]. Bdnf is expressed in the neocortex throughout brain development[39] and has been reported to accelerate overall redistribution of cortical neurons[40].

These observations suggested that Bdnf may explain some of the more unusual aspects of the Kif1a knockdown phenotype. To test this possibility, we performed Bdnf RNAi by *in utero* electroporation at E16. By E20, we observed an accumulation of multipolar neurons in the SVZ and lower IZ (**Fig. 8a**,**b**), comparable to the effects of Kif1a RNAi. Moreover, most of the Bdnf-depleted and nearby non-electroporated multipolar neurons ectopically expressed Tbr1 (**Fig. 8a**), phenocopying the non-cell-autonomous effect of Kif1a RNAi. However, by P7 we saw no clear accumulation of non-transfected cells in the white matter or ectopic accumulation of the late neuronal marker CDP. These results suggest either less complete inhibition of migration by Bdnf versus Kif1a RNAi or a contribution of other Kif1a-dependent neurotrophic factors at postnatal stages of development. We also tested the effects of Bdnf RNAi on nuclear migration in RGP cells, which appeared to be normal, as the distribution of nuclei near the VS in fixed brain sections was comparable to controls (**Fig. 8c**).

We then treated E19 Kif1a knockdown slices with recombinant BDNF (50 ng ml^{-1}; **Fig. 8d**)[41]. Neurons expressing Kif1a RNAi were still arrested in the SVZ and IZ at the multipolar stage, although they no longer expressed Tbr1, as in normal cells. Notably, BDNF application reversed the non-cell-autonomous Tbr1 staining in control cells in the SVZ and lower IZ, and was restored to its normal distribution as a band in the CP. The region of Tbr1 staining was, however, thinner and more superficially located than in control brain, suggesting that migrating cells travel faster and/or further in the presence of excess BDNF. We also tested the effects of BDNF after depletion of Kif1a specifically in neurons and on cells expressing the KIF1A R18W mutant (**Supplementary Fig. 6b**,**c**). In both cases, BDNF again failed to reverse the migratory and morphogenetic arrest of the transfected

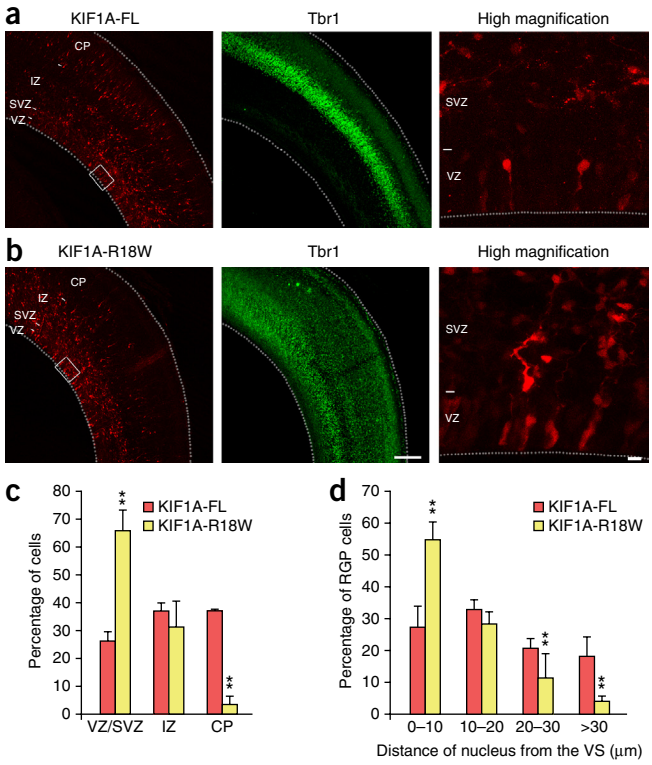

Figure 7 Effect of KIF1A R18W human mutation on INM and neuronal migration. (**a**,**b**) Coronal sections of E20 rat brains electroporated at E16 with cDNAs encoding the human wild-type, KIF1A-FL (**a**), or the human mutant form of KIF1A, KIF1A-R18W (**b**). Expression of KIF1A-R18W resulted in a defect in INM, as evidenced by the close proximity of nuclei to the ventricular surface (high magnification), in neuronal migration, as indicated by the accumulation of neurons in the SVZ and lower IZ, and a non-cell-autonomous effect on neighboring cells as revealed by ectopic Tbr1 staining in these regions (high magnification). (**c**) Quantification of cell distribution in the cortex at E20 (VZ/SVZ: KIF1A-FL, 26.18 ± 3.3%; KIF1A-R18W, 65.48 ± 7.4%; IZ: KIF1A-FL, 36.91 ± 2.6%; KIF1A-R18W, 31.32 ± 9%; CP: KIF1A-FL, 36.89 ± 0.7%; KIF1A-R18W, 3.1 ± 3.1%; $n = 5$ KIF1A-FL and 6 KIF1A-R18W) showing a significant increase of mutant cells in SVZ and lower IZ. (**d**) Quantification of the distance of RGP nuclei from the VS at E20 (0–10: KIF1A-FL, 25.76 ± 5.5%; KIF1A-R18W, 55.2 ± 5.4%; 10–20: KIF1A-FL, 33.37 ± 2.2%; KIF1A-R18W, 28.75 ± 3.3%; 20–30: KIF1A-FL, 21.47 ± 2%; KIF1A-R18W, 11.74 ± 7.6%; >30: KIF1A-FL, 19.17 ± 4.4%; KIF1A-R18W, 4.3 ± 1.3%; $n = 5$ KIF1A-FL and 6 KIF1A-R18W), revealing accumulation at this site for the mutant, but not wild-type, KIF1A. $^*P < 0.05$, $^{**}P < 0.01$ (VZ/SVZ, $P = 0.0043$; IZ, $P = 0.329$; CP, $P = 0.0043$; 0–10, $P = 0.0043$; 10–20, $P = 0.0303$; 20–30, $P = 0.0087$; >30, $P = 0.0043$). Error bars represent mean ± s.d. Scale bars represent 100 μm (**a**,**b**, left two panels) and 15 μm (high magnification in **a**,**b**).

cells, although Tbr1 expression was blocked and the non-autonomous effect on surrounding cells was eliminated. We also analyzed Bdnf knockdown brains at P7, where we again observed an accumulation of the transfected cells in what was now the white matter, but a dispersed distribution of individual cells throughout the cortical layers (**Supplementary Fig. 7c**).

Together, these data suggest that BDNF contributes to the non-cell-autonomous effects of Kif1a knockdown, likely in its role as a diffusible neurotrophic agent. As a further test of this possibility, we performed RNAi for the BDNF receptor TrkB. We again observed an accumulation of knockdown cells in the SVZ and lower IZ (**Supplementary Fig. 3e**). However, there was no indication of a non-cell-autonomous effect on surrounding control cells in this region, as judged by the absence of ectopic Tbr1 expression.

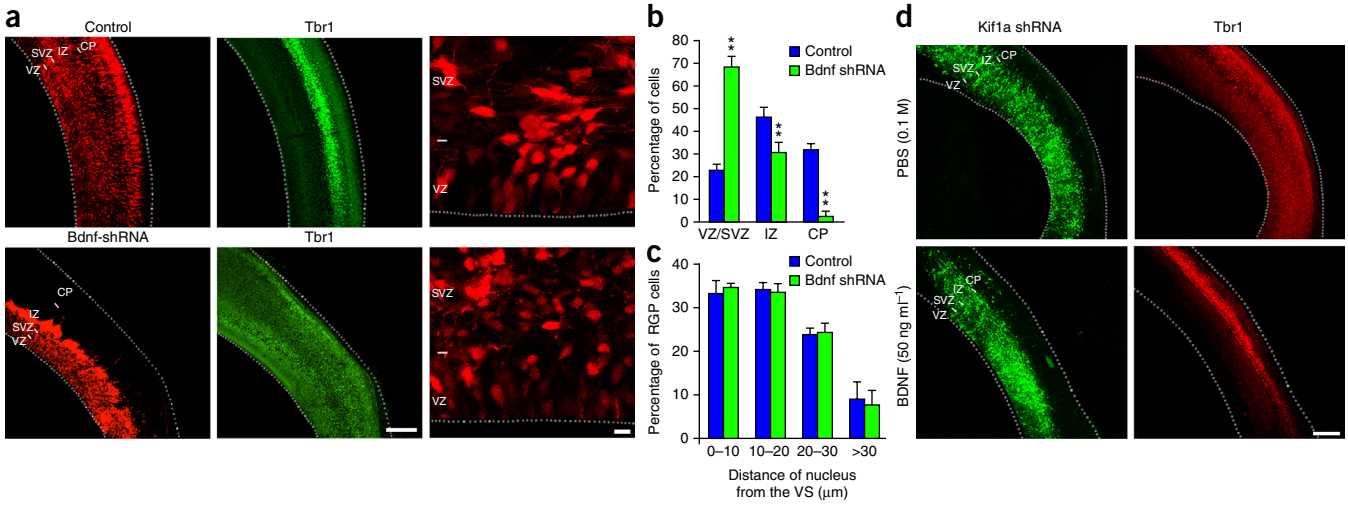

Figure 8 Role of BDNF in KIF1A pathway. (**a**) E20 coronal sections of rat brains electroporated at E16 with BDNF shRNA. BDNF knockdown resulted in a potent accumulation of neurons in the SVZ and lower IZ (high magnification), as well as ectopic expression of Tbr1 throughout this region, comparable to the effects of Kif1a RNAi. (**b**) Quantification of data in A (VZ/SVZ: control, 22.54 ± 2.3%; Bdnf shRNA, 68.12 ± 4.7%; IZ: control, 45.91 ± 4.1%; Bdnf shRNA, 30.13 ± 5%; CP: control, 31.54 ± 3.2%; Bdnf shRNA, 1.7 ± 2.5%; $n = 6$). (**c**) Quantification of the distance of RGP nuclei from the VS at E20 (0–10: control, 33.17 ± 3%; Bdnf shRNA, 34.6 ± 1.1%; 10–20: control, 34.04 ± 1.5%; Bdnf shRNA, 33.5 ± 2.1%; 20–30: control, 23.8 ± 1.4%; Bdnf shRNA, 24.12 ± 2.4%; >30: control, 9 ± 4%; Bdnf shRNA 7.75 ± 3.2%; $n = 4$ control and 7 Bdnf shRNA), revealing no INM defect after Bdnf depletion. (**d**) E19 coronal rat brain slices cultured for 24 h in the presence of recombinant BDNF (50 ng ml^{-1}) in phosphate-buffered saline (PBS), or control vehicle alone, and then fixed and examined by microscopy. BDNF treatment rescued the non-cell-autonomous effect caused by Kif1a shRNA, as evidenced by restoration of migration in non-transfected cells and normal Tbr1 distribution. $^{**}P < 0.01$ (VZ/SVZ, IZ and CP: $P = 0.0022$; 0–10: $P = 0.3818$; 10–20: $P = 0.7818$; 20–30: $P > 0.9999$; >30: $P = 0.4424$). Error bars represent mean ± s.d. Scale bars represent 100 μm (**a**, left two panels; **d**) and 15 μm (**a**, right panel).

These results also suggest that BDNF treatment can be used as an additional test for a common Kif1a-Bdnf-Dcx pathway. We found that BDNF application to brain slices from Dcx knockdown rats completely reversed the non-cell-autonomous accumulation of multipolar cells in the SVZ and lower IZ and ectopic expression of Tbr1 in these and the Dcx knockdown cells (**Supplementary Fig. 6a**).

Bdnf shRNA caused no change in cell fate, as judged by immunostaining with Pax6 (RGPs) and TuJ1 (neurons; Pax6: control, 19.33 ± 5.1%, n = 4; Bdnf shRNA, 15.96 ± 3.2%, P = 0.3429, n = 4; Tuj1: control, 45.83 ± 4.1%, n = 5; Bdnf shRNA, 48.17 ± 4.7%, n = 4, P = 0.4127; **Supplementary Fig. 7a**,**b**). Finally, BDNF application failed to rescue INM in Kif1a-depleted brain sections (**Supplementary Fig. 6d**,**e**). Together, these results argue that BDNF has a critical role in postmitotic neuronal migration, but not in the earlier steps of brain development.

DISCUSSION

Our earlier work revealed that Kif1a RNAi specifically blocks basal INM in RGP cells[9] and decreases neuronal number, but the relationship between these effects remains unclear. Here we found that cell cycle progression persisted even when basal INM was blocked, but self-renewing divisions were greatly increased (**Supplementary Fig. 7e**). The remaining postmitotic neurons arrested in the SVZ and IZ at the multipolar-to-bipolar transition while expressing later differentiation markers and potently altering morphogenesis and gene expression in surrounding non-transfected cells. These effects were mimicked by Dcx and Bdnf RNAi and rescued by BDNF application, providing insight into an emerging brain developmental pathway.

Consequences of basal INM inhibition

INM has long known to be entrained with RGP cell cycle progression, but cell cycle control of INM and vice versa remains only partially explored. We previously found that blocking apical INM prevents mitotic entry[10], providing clear evidence that nuclear position controls the G2-M transition. We found the effects of Kif1a inhibition to be quite different. Kif1a RNAi and expression of the R18W mutant caused clear accumulation of nuclei at or near the ventricle in the developing neocortex. Cell cycle progression persisted, however, as judged by normal or near-normal numbers of cells in G1, S and M phase. Particularly noteworthy was the unusual presence of BrDU-positive nuclei near or at the VS (**Fig. 1e**–**g**). S phase normally occurs at a distance from the ventricle, but our data suggest that DNA replication is actually free of spatial constraint.

Although Kif1a RNAi had little cell cycle effect, the ratio of asymmetric-to-symmetric RGP cell divisions decreased markedly, as judged by live mitotic behavior. This effect may well contribute to the increase in RGP cells and decrease that we observed in neurons generated in Kif1a knockdown brain[9].

The decrease in neurogenic divisions might, conceivably, reflect increased exposure of RGP nuclei to proliferative signals near or decreased exposure to differentiative signals away from the VS[42]. In this view, mitotic spindle orientation might be an indirect consequence of nuclear exposure to environmental cues.

Alternatively, as a microtubule motor protein, KIF1A might affect spindle orientation or other aspects of the mitotic process. KIF1A is currently known exclusively for its interphase roles in vesicular transport and, in our hands, nuclear migration. However, the marked change in cell division plane that we observed could reflect a previously unknown KIF1A contribution to spindle positioning.

A major function of INM may be to accommodate more cycling cells in the VZ[43], a possibility made more compelling by the restriction of mitotic entry to the VS[10]. RNAi-mediated inhibition of basal INM could increase crowding near the VS and may, in part, account for the modest displacement of apparently immotile nuclei from the VS that we observed (**Fig. 2**). However, the small fraction of RGP cell bodies displaced as a result of Kif1a shRNA might be insufficient to block nuclei from reaching the VS for timely mitotic entry.

Exit from the multipolar stage requires Kif1a

A notable developmental effect of Kif1a RNAi was the accumulation of multipolar neurons in the SVZ and lower IZ. Our data suggest that this result is independent of altered INM (**Fig. 6**), and is instead intrinsic to postmitotic neurons. The developmental purpose of the multipolar stage and the mechanisms underlying transition to the bipolar migratory stage are incompletely understood, but our data implicate KIF1A in this process. We found that the multipolar stage may persist for several days in control cells, but much longer under conditions of reduced Kif1a expression or following expression of mutant KIF1A. Despite the near-complete inability of the knockdown multipolar cells to exit this stage, a few bipolar-shaped Kif1a-depleted cells did reach the lower IZ and the CP. Based on our analysis of the multipolar-to-bipolar transition, we suspect that these neurons must be only partially inhibited for Kif1a expression. Based on our previous studies of the dynein pathway[9,10,14], we propose that KIF1A and dynein contribute to a common, major morphogenetic transition, although, given the opposite direction for force production by these motor proteins, their specific molecular roles must be distinct.

Ectopic expression of late neuronal markers in Kif1a knockdown cells

Another aspect of the Kif1a RNAi phenotype is the expression of the mature neuronal markers Tbr1, NeuN and CDP in the arrested multipolar cells. The markers appeared in normal temporal sequence, suggesting a failure in mechanisms coordinating morphogenesis with gene expression. This aspect of the Kif1a phenotype also contrasts with the results of RNAi for dynein-related proteins, which arrests cells at the multipolar stage without expression of Tbr1 (**Supplementary Fig. 3a**–**c**). The basis for this difference will require further studies to elucidate.

Non-cell-autonomous effects of altered Kif1a expression

Equally notable is the non-cell-autonomous aspect of the Kif1a RNAi phenotype. As for the knockdown cells themselves, neighboring non-transfected cells in the SVZ and lower IZ were morphogenetically delayed at the multipolar stage, but still expressed late neuronal markers. This again differed from the effects of RNAi for dynein-related genes (**Supplementary Fig. 3a**–**c**), which had no apparent effect on nearby control cells and seemed to arrest the neuronal gene expression program.

We envision that the non-cell-autonomous effect of Kif1a RNAi may involve either physical or chemical modes of intercellular communication. Theoretically, entanglement of the multiple processes of adjacent cells in the SVZ and lower IZ might restrain non-transfected cells from migrating, though lack of such an effect for dynein-related genes argues against this model.

Direct communication among multipolar cells by secreted factors represents another possibility, and our results strongly implicate BDNF in cell-cell communication in the SVZ. KIF1A- and BDNF-positive vesicles were reported to co-migrate in axons, and the transport of the latter was affected by Kif1a RNAi[37]. We therefore reasoned that BDNF secretion in the SVZ might be affected by altered KIF1A expression. To test this possibility, we performed Bdnf RNAi, which

mimicked the effects of Kif1a RNAi, a sign that these genes function in a common pathway. We also applied BDNF to rat brain slices, which rescued much of the Kif1a RNAi phenotype, including the non-cell-autonomous effects. The Kif1a-depleted cells no longer expressed ectopic Tbr1, although they did remain arrested in the SVZ and lower IZ with a multipolar morphology. This result may indicate a separate BDNF-independent role for KIF1A in morphogenesis.

Overall, we suggest that BDNF has an autocrine effect on postmitotic neurons and a paracrine effect to coordinate the behavior of surrounding neurons. This hypothesis is supported by the strictly cell-autonomous effect of TrkB RNAi, the effect of which should be to interfere solely with BDNF intake in the knockdown cell.

Although Bdnf RNAi completely phenocopied the effects of Kif1a RNAi on postmitotic neurons examined at E20, the consequences of Bdnf RNAi appeared less severe by P7. This could reflect less efficient inhibition of Bdnf versus Kif1a or a decreased importance for BDNF during postnatal development. This reasoning is consistent with the phenotype observed in a Bdnf conditional knockout mouse, in which there was no gross disruption of cortical layers in 5-week-old mice[44].

We observed no effect of Bdnf RNAi on INM, and applied BDNF did not rescue the INM defect caused by Kif1a RNAi. Consistent with these results, Bdnf RNAi had no apparent effect on cell fate.

Relationship among KIF1A, DCX and BDNF

Several of the effects of Kif1a RNAi and the p.R18W mutation are reminiscent of the RNAi phenotype for Dcx, which was reported to interact with Kif1a[20]. The initial report of Dcx RNAi effects involved an accumulation of neurons in the SVZ[33]. This effect was seen in nearby independently transfected control cells[33], but the importance of this behavior has not been investigated further. Here we characterized the Dcx RNAi phenotype in more detail. The consequences for postmitotic neurons, including ectopic gene expression, are markedly similar to those we identified for Kif1a. Equally important, the effects of BDNF application are essentially identical for both Kif1a and Dcx knockdown cells.

Basis for KIF1A-mediated cortical malformations

A patient harboring a *de novo* KIF1A motor domain mutation, p.R18W, exhibited frontal pachygyria, a thick corpus callosum and reduction of white matter[27]. Upon expressing a human KIF1A R18W cDNA in rat brain progenitors *in utero* (**Fig. 7**), we observed clear defects in both neuronal migration and basal INM. We speculate that the dominant effect of the cDNA reflects the ability of the mutant polypeptide to form heterodimers with the endogenous wild-type protein.

METHODS

Methods and any associated references are available in the online version of the paper.

Note: Any Supplementary Information and Source Data files are available in the online version of the paper.

ACKNOWLEDGMENTS

We thank F. Polleux, H. Wichterle, J. Goldman and T. Dantas for critical reading and input to our manuscript. We thank G. Krietzer (Cell and Developmental Biology, Weill Cornell Medical College), C. Cardoso and A. Falace (Institut de Neurobiologie de la Méditerranée INSERM UMR901) for reagents. We thank A. Represa, C. Pellegrino and D. Doobin for advice. This project was supported by US National Institutes of Health grant HD40182 to R.B.V.

AUTHOR CONTRIBUTIONS

A.C. and R.B.V. conceived the project and wrote the manuscript. A.C. and D.J.-K.H. performed experiments and analyzed data. All of the authors read and approved the final manuscript.

COMPETING FINANCIAL INTERESTS

The authors declare no competing financial interests.

1. Kosodo, Y. Interkinetic nuclear migration: beyond a hallmark of neurogenesis. *Cell. Mol. Life Sci.* **69**, 2727–2738 (2012).
2. Taverna, E. & Huttner, W.B. Neural progenitor nuclei IN motion. *Neuron* **67**, 906–914 (2010).
3. Spear, P.C. & Erickson, C.A. Interkinetic nuclear migration: a mysterious process in search of a function. *Dev. Growth Differ.* **54**, 306–316 (2012).
4. Kriegstein, A. & Alvarez-Buylla, A. The glial nature of embryonic and adult neural stem cells. *Annu. Rev. Neurosci.* **32**, 149–184 (2009).
5. Noctor, S.C., Flint, A.C., Weissman, T.A., Dammerman, R.S. & Kriegstein, A.R. Neurons derived from radial glial cells establish radial units in neocortex. *Nature* **409**, 714–720 (2001).
6. Paridaen, J.T.M.L. & Huttner, W.B. Neurogenesis during development of the vertebrate central nervous system. *EMBO Rep.* **15**, 351–364 (2014).
7. Noctor, S.C., Martínez-Cerdeño, V., Ivic, L. & Kriegstein, A.R. Cortical neurons arise in symmetric and asymmetric division zones and migrate through specific phases. *Nat. Neurosci.* **7**, 136–144 (2004).
8. LoTurco, J.J. & Bai, J. The multipolar stage and disruptions in neuronal migration. *Trends Neurosci.* **29**, 407–413 (2006).
9. Tsai, J.-W., Lian, W.-N., Kemal, S., Kriegstein, A.R. & Vallee, R.B. Kinesin 3 and cytoplasmic dynein mediate interkinetic nuclear migration in neural stem cells. *Nat. Neurosci.* **13**, 1463–1471 (2010).
10. Hu, D.J.-K. *et al.* Dynein recruitment to nuclear pores activates apical nuclear migration and mitotic entry in brain progenitor cells. *Cell* **154**, 1300–1313 (2013).
11. Norden, C., Young, S., Link, B.A. & Harris, W.A. Actomyosin is the main driver of interkinetic nuclear migration in the retina. *Cell* **138**, 1195–1208 (2009).
12. Meyer, E.J., Ikmi, A. & Gibson, M.C. Interkinetic nuclear migration is a broadly conserved feature of cell division in pseudostratified epithelia. *Curr. Biol.* **21**, 485–491 (2011).
13. Schenk, J., Wilsch-Bräuninger, M., Calegari, F. & Huttner, W.B. Myosin II is required for interkinetic nuclear migration of neural progenitors. *Proc. Natl. Acad. Sci. USA* **106**, 16487–16492 (2009).
14. Tsai, J.-W., Chen, Y., Kriegstein, A.R. & Vallee, R.B. LIS1 RNA interference blocks neural stem cell division, morphogenesis, and motility at multiple stages. *J. Cell Biol.* **170**, 935–945 (2005).
15. Lipka, J., Kuijpers, M., Jaworski, J. & Hoogenraad, C.C. Mutations in cytoplasmic dynein and its regulators cause malformations of cortical development and neurodegenerative diseases. *Biochem. Soc. Trans.* **41**, 1605–1612 (2013).
16. Poirier, K. *et al.* Mutations in TUBG1, DYNC1H1, KIF5C and KIF2A cause malformations of cortical development and microcephaly. *Nat. Genet.* **45**, 639–647 (2013).
17. Alkuraya, F.S. *et al.* Human mutations in NDE1 cause extreme microcephaly with lissencephaly [corrected]. *Am. J. Hum. Genet.* **88**, 536–547 (2011).
18. Fiorillo, C. *et al.* Novel dynein DYNC1H1 neck and motor domain mutations link distal spinal muscular atrophy and abnormal cortical development. *Hum. Mutat.* **35**, 298–302 (2014).
19. Dobyns, W.B., Reiner, O., Carrozzo, R. & Ledbetter, D.H. Lissencephaly. A human brain malformation associated with deletion of the LIS1 gene located at chromosome 17p13. *J. Am. Med. Assoc.* **270**, 2838–2842 (1993).
20. Liu, J.S. *et al.* Molecular basis for specific regulation of neuronal kinesin-3 motors by doublecortin family proteins. *Mol. Cell* **47**, 707–721 (2012).
21. Yonekawa, Y. *et al.* Defect in synaptic vesicle precursor transport and neuronal cell death in KIF1A motor protein-deficient mice. *J. Cell Biol.* **141**, 431–441 (1998).
22. Klebe, S. *et al.* Autosomal recessive spastic paraplegia (SPG30) with mild ataxia and sensory neuropathy maps to chromosome 2q37.3. *Brain* **129**, 1456–1462 (2006).
23. Erlich, Y. *et al.* Exome sequencing and disease-network analysis of a single family implicate a mutation in KIF1A in hereditary spastic paraparesis. *Genome Res.* **21**, 658–664 (2011).
24. Klebe, S. *et al.* KIF1A missense mutations in SPG30, an autosomal recessive spastic paraplegia: distinct phenotypes according to the nature of the mutations. *Eur. J. Hum. Genet.* **20**, 645–649 (2012).
25. Rivière, J.-B. *et al.* KIF1A, an axonal transporter of synaptic vesicles, is mutated in hereditary sensory and autonomic neuropathy type 2. *Am. J. Hum. Genet.* **89**, 219–230 (2011).
26. Hamdan, F.F. *et al.* S2D Group. Excess of *de novo* deleterious mutations in genes associated with glutamatergic systems in nonsyndromic intellectual disability. *Am. J. Hum. Genet.* **88**, 306–316 (2011).
27. Jamuar, S.S. *et al.* Somatic mutations in cerebral cortical malformations. *N. Engl. J. Med.* **371**, 733–743 (2014).
28. Esmaeeli Nieh, S. *et al. De novo* mutations in KIF1A cause progressive encephalopathy and brain atrophy. *Ann. Clin. Transl. Neurol.* **2**, 623–635 (2015).
29. Kosodo, Y. *et al.* Regulation of interkinetic nuclear migration by cell cycle–coupled active and passive mechanisms in the developing brain. *EMBO J.* **30**, 1690–1704 (2011).

30. Bedogni, F. *et al.* Tbr1 regulates regional and laminar identity of postmitotic neurons in developing neocortex. *Proc. Natl. Acad. Sci. USA* **107**, 13129–13134 (2010).
31. Englund, C. *et al.* Pax6, Tbr2, and Tbr1 are expressed sequentially by radial glia, intermediate progenitor cells, and postmitotic neurons in developing neocortex. *J. Neurosci.* **25**, 247–251 (2005).
32. Ye, T., Ip, J.P.K., Fu, A.K.Y. & Ip, N.Y. Cdk5-mediated phosphorylation of RapGEF2 controls neuronal migration in the developing cerebral cortex. *Nat. Commun.* **5**, 4826 (2014).
33. Bai, J. *et al.* RNAi reveals doublecortin is required for radial migration in rat neocortex. *Nat. Neurosci.* **6**, 1277–1283 (2003).
34. Carabalona, A. *et al.* A glial origin for periventricular nodular heterotopia caused by impaired expression of Filamin-A. *Hum. Mol. Genet.* **21**, 1004–1017 (2012).
35. Xue, X., Jaulin, F., Espenel, C. & Kreitzer, G. PH-domain-dependent selective transport of p75 by kinesin-3 family motors in non-polarized MDCK cells. *J. Cell Sci.* **123**, 1732–1741 (2010).
36. Okada, Y., Yamazaki, H., Sekine-Aizawa, Y. & Hirokawa, N. The neuron-specific kinesin superfamily protein KIF1A is a unique monomeric motor for anterograde axonal transport of synaptic vesicle precursors. *Cell* **81**, 769–780 (1995).
37. Lo, K.Y., Kuzmin, A., Unger, S.M., Petersen, J.D. & Silverman, M.A. KIF1A is the primary anterograde motor protein required for the axonal transport of dense-core vesicles in cultured hippocampal neurons. *Neurosci. Lett.* **491**, 168–173 (2011).
38. Kondo, M., Takei, Y. & Hirokawa, N. Motor protein KIF1A is essential for hippocampal synaptogenesis and learning enhancement in an enriched environment. *Neuron* **73**, 743–757 (2012).
39. Fukumitsu, H. *et al.* Simultaneous expression of brain-derived neurotrophic factor and neurotrophin-3 in Cajal-Retzius, subplate and ventricular progenitor cells during early development stages of the rat cerebral cortex. *Neuroscience* **84**, 115–127 (1998).
40. Behar, T.N. *et al.* Neurotrophins stimulate chemotaxis of embryonic cortical neurons. *Eur. J. Neurosci.* **9**, 2561–2570 (1997).
41. Polleux, F., Whitford, K.L., Dijkhuizen, P.A., Vitalis, T. & Ghosh, A. Control of cortical interneuron migration by neurotrophins and PI3-kinase signaling. *Development* **129**, 3147–3160 (2002).
42. Del Bene, F., Wehman, A.M., Link, B.A. & Baier, H. Regulation of neurogenesis by interkinetic nuclear migration through an apical-basal notch gradient. *Cell* **134**, 1055–1065 (2008).
43. Florio, M. & Huttner, W.B. Neural progenitors, neurogenesis and the evolution of the neocortex. *Development* **141**, 2182–2194 (2014).
44. Gorski, J.A., Zeiler, S.R., Tamowski, S. & Jones, K.R. Brain-derived neurotrophic factor is required for the maintenance of cortical dendrites. *J. Neurosci.* **23**, 6856–6865 (2003).

ONLINE METHODS

RNAi and dominant-negative construct. We used two different shRNA for Kif1a[9]. Those shRNA were subcloned in different vectors: for the embryonic experiment, Kif1a-shRNA was cloned into the pRNAT-U6.1/Neo (GenScript) as it was reported previously[9]; for the postnatal experiments the two different shRNA were subcloned into an mU6pro vector[45]; for the conditional experiment we cloned the miR30-based Kif1a shRNA in the pCALSL-mir30 vector (Addgene plasmid 13786 (ref. 46); primers: forward, 5′- TCGAGAAGGTATATTGCTGT TGACAGTGAGCGCTTGGCGAT ATCACTGACATGATAGTGAAGCCACA GATGTATCATGTCAGTGATATCGCCAAGTGCCTACTGCCTCGG-3′; and reverse, 5′-AATTCCGAGGCAGTAGGCACTTGGCGATATCACTGACATGA TACATCTGTGGCTTCACT ATCATGTCAGTGATATCGCCAAGCGCTCAC TGTCAACAGCAATATACCTTC-3′) and co-transfected with BLBP-cre-GFP or the NeuroD-cre with pCAG-RFP. The dominant negative construct KIF1A-R18W was made by PCR mutagenesis (primers: forward, 5′-GGGTCCGCCCCTTCA ATTCCTGGGAAATGAGCCGTGACTCCAA-3′; and reverse, 5′-TTGGAGTCA CGGCTCATTTCCCAGGAATTGAAGGGGCGGACCC-3′) using the KOD Hot Start DNA Polymerase Kit, according to the manufacturer's protocol (Millipore). Bdnf shRNA[47] and TrkB shRNA[48] were subcloned into the mU6pro vector.

***In utero* electroporation.** Plasmids or oligonucleotides were transfected using intraventricular injection followed by *in utero* electroporation[49,50]. In brief, timed pregnant Sprague Dawley rats (Taconic; E16; E1 was defined as the day of confirmation of sperm-positive vaginal plug) were anesthetized with a mixture of ketamine/xylazine (respectively at 90 and 5 mg per kg of body weight). For pain management, bupivacaine (2 mg per kg) was administered via a subcutaneous injection at the site of the future incision, and buprenorphine (0.05 mg per kg) was administered by a subcutaneous injection. This dose of buprenorphine was re-administered to the animal every 8–12 h, for up to 48 h following the surgery. The lateral ventricle of each embryo was injected with Fast Green (2 mg ml^{-1}; Sigma) combined with shRNA (1.5 μg $μl^{-1}$). Plasmids were further electroporated by discharging a 4,000-mF capacitor charged to 50V with a BTX ECM 830 electroporator (BTX Harvard Apparatus). The voltage was discharged in five electrical pulses at 950-ms intervals via 7-mm electrodes placed on the head of the embryo across the uterine wall. For P7 experiments, animals were designated as P0 on day of birth (generally around E22). For sequential electroporation experiments, we introduced a cDNA encoding pCAG-RFP into E16 rat brain, followed 30 min later by a plasmid coexpressing GFP plus scrambled or Kif1a shRNA (we note that the number of RFP+ cells is greater than the number of GFP+ cells because of the difference in promotors). Animals were maintained according to protocols approved by the Institutional Animal Care and Use Committee at Columbia University. In general, embryonic rats experience a 1.5–2-d delay in development compared to embryonic mice. Therefore, E16, E19 and E20 rats are approximately equivalent to E14.5, E17.5 and E18.5 respectively (with E1 defined as the day of confirmation of sperm-positive vaginal plug). The number of animals has been calculated on the basis of the requirement for adequate numbers of brain slices and sections for sufficient imaging to provide statistically significant data on the effects of RNAi, small molecules, and other reagents used in the proposed analysis, plus controls.

Live imaging. E20 dissected rat brains were transferred in 4% (in artificial cerebrospinal fluid) low melting agarose in plastic embedding molds, and were sectioned coronally (300 μm) on a vibratome (Leica Microsystems). Slices were placed on 0.4-μm, 30-mm diameter Millicell-CM inserts (Millipore) in cortical culture medium containing 25% Hanks balanced salt solution, 47% basal MEM, 25% normal horse serum, 1× penicillin/streptomycin/glutamine (GIBCO BRL), and 30% glucose. Slice was transferred to a 50-mm glass-bottom dish and was imaged on an IX80 laser scanning confocal microscope (Olympus FV100 Spectral Confocal System) at intervals of 15 min for 48 h.

Immunostaining of brain slices. Rat brains were fixed (E20) or perfused (P7) transcardially with chilled saline and 4% paraformaldehyde (PFA; EMS, wt/vol) and then incubated in 4% PFA overnight. Brain slices were sectioned coronally (100 μm) on a vibratome (Leica Microsystems). Brain slices were washed with PBS (pH 7.4) and stained in PBS 0.3% Triton X-100 supplemented with 5% of donkey serum. Primary antibodies were incubated overnight at 4 °C, sections were then washed with PBS and incubated in secondary antibodies for 2 h at 22–25 °C. For BrDU labeling experiments, BrDU (Sigma-Aldrich, B5002) was injected at 50 mg per kg body weight intra-peritoneally 20 min before embryo harvest, then, brain slices were first incubated in 2N HCl for 25 min at 37 °C, and then washed in PBS before antibody incubation. Antibodies used in this study were: Tbr2 (Millipore, AB2283), KI67 (Millipore, AB9260), Geminin (Santa-Cruz, SC-13015), Tbr1 (Abcam, ab31940), CDP (Santa-Cruz, SC-13024), NeuN (Millipore, MAB377), Cyclin D1 (ThermoScientific, RM-9104-S0), phospho-histone H3 (Abcam, ab14955), BrDU (Abcam, ab6326), Vimentin (Millipore, MAB3400).

Pharmacology. Brains were sliced and prepared as detailed in the live imaging protocol. 300-μm slices were transferred to 0.4-μm, 30-mm diameter filters and incubated in 1 ml of cortical culture medium containing BDNF (Sigma, B3795, 50 ng ml^{-1}, diluted in PBS pH 7.4), overnight in a 37 °C incubator with 5% CO_2. For immunostaining, slices were fixed in PFA (overnight at 4 °C) and incubated with Tbr1 antibody overnight at 4 °C, sections were then washed with PBS and incubated in secondary antibody for 2 h at 22–25 °C.

Microscopy and image analysis. All images were collected with an IX80 laser scanning confocal microscope (Olympus FV100 Spectral Confocal System). Brain sections were imaged using a 60× 1.42 N.A. oil objective or a 10× 0.40 N.A. air objective. All images were analyzed using ImageJ (US National Institutes of Health). P7 coronal sections were imaged at 60× and the heterotopia size was estimated in square-pixel with the ImageJ polygon tool and converted to mm^2. In the defined area, using the ImageJ plugin Cell Counter, we calculated the number of transfected and non-transfected cells that were positive for NeuN and CDP markers.

Statistical data. In each experiment, *n* represents the number of brains from at least three different mothers. Statistical analyses were performed with Prism (GraphPad Software). A two-sample Student's *t* test was used to compare means of two independent groups if the distribution of the data was normal. If the values come from a Gaussian distribution (D'agostino-Pearson omnibus normality test) the parametric unpaired *t* test with Welch's correction was used. But, when the normality test failed, the non-parametric Mann-Whitney test was used. Significance was accepted at the level of $P < 0.05$.

No statistical methods were used to predetermine sample sizes, but our sample sizes are similar to those generally employed in the field. No randomization was used to collect all the data, but they were quantified blindly.

A **Supplementary Methods Checklist** is available.

45. Yu, J.-Y., DeRuiter, S.L. & Turner, D.L. RNA interference by expression of short-interfering RNAs and hairpin RNAs in mammalian cells. *Proc. Natl. Acad. Sci. USA* **99**, 6047–6052 (2002).
46. Matsuda, T. & Cepko, C.L. Controlled expression of transgenes introduced by in vivo electroporation. *Proc. Natl. Acad. Sci. USA* **104**, 1027–1032 (2007).
47. Taliaz, D., Stall, N., Dar, D.E. & Zangen, A. Knockdown of brain-derived neurotrophic factor in specific brain sites precipitates behaviors associated with depression and reduces neurogenesis. *Mol. Psychiatry* **15**, 80–92 (2010).
48. Zhao, C.-T. *et al.* PKCdelta regulates cortical radial migration by stabilizing the Cdk5 activator p35. *Proc. Natl. Acad. Sci. USA* **106**, 21353–21358 (2009).
49. Saito, T. & Nakatsuji, N. Efficient gene transfer into the embryonic mouse brain using *in vivo* electroporation. *Dev. Biol.* **240**, 237–246 (2001).
50. Tabata, H. & Nakajima, K. Efficient in utero gene transfer system to the developing mouse brain using electroporation: visualization of neuronal migration in the developing cortex. *Neuroscience* **103**, 865–872 (2001).